CONF-8610115--4

Presented at the
IV International Symposium on the Production and Neutralization of Negative Ions and Beams
Brookhaven National Laboratory
October 27-31, 1986

FUNDAMENTAL PROCESSES IN LOW ENERGY COLLISIONS OF ALKALI ANIONS AND ATOMS

CONF-8610115--

DE87 002705

R.L. Champion, L.D. Doverspike, D.M. Scott, and Yicheng Wang
Department of Physics, College of William and Mary
Williamsburg, VA 23185, USA

I. INTRODUCTION

Negative ion sources often employ alkali metal atoms in one way or another in order to increase their yield. Models which describe equilibrium conditions or the nature of energy transport within these sources require, among other things, information about the two-body cross sections for various scattering channels which involve either alkali negative ions or alkali atoms. The purpose of this report is to provide a brief summary of recent experimental observations in which collisions of alkali anions (M^-) with various atoms and molecules and collisions of H^- and D^- with alkali atoms (M) have been investigated. The energy range of the experiments, $5 < E < 500$ eV, includes those kinetic energies often found in discharge-type ion sources. The specific experiments which will be discussed focus upon measurements of total cross sections for collisional electron detachment and charge transfer of negative ions.

II. EXPERIMENTAL METHODS

Experiments which involve alkali negative ion beams or alkali atomic beams have problems associated with the handling, etc., of alkali metals and it is perhaps of interest to discuss those relevant features of the two types of experiments, $M^- + X$ and $H^- + M$.

The alkali negative ions, Cs^-, K^-, and Na^- are produced in a discharge-type source whose design is based upon the observation of K^- production by electrical discharges in potassium vapor at low pressure[1] (0.01 - 0.3 torr). In the present source,[2,3] the discharge is maintained in a pure alkali vapor; the source and oven temperatures at which the yield is maximum imply that the principal mechanism for M^- production may be via dissociative attachment to alkali dimers. The oven which supplies the source is maintained at 230C, 250C and 300C for Cs, K, and Na, respectively; the source is maintained at 350C for all three alkali metals.

The performance of this source is adequate for these experiments: typical mass-analyzed currents produced are 0.11 nA of Na^-, 0.45 nA of K^-, and 0.5 nA of Cs^-. The energy width of these beams can be as low as 0.2 eV and is generally less than 1 eV.

It has been observed that this ion source produces anions with

masses corresponding to NaH^- and KH^-. During the first several hours of operation, the hydride ions are more abundant than the desired alkali-metal anion, but the mass peak associated with the hydrides diminishes with the time. These hydrides are thought to result from reactions of the alkali-metals with water vapor present in the source. In order to ensure that there are no undesired ions in the primary beam, a 90° double-focusing section magnet with a resolution of 1% has been employed for mass analysis. The K^- and KH^- mass peaks are clearly resolved; the observed contamination of the K^- primary beam by KH^- is less than 1%. The Na^- and Cs^- beams are similarly pure.

The beam of alkali anions is directed into a collision region which contains a gas-phase target; σ_e and σ_{ct} are measured by separating and trapping the detached electrons and the (relatively slow) charge transfer products.[4]

A gaseous target can not be employed for studies of alkali atomic targets; rather a crossed beam apparatus has been constructed for that purpose. A schematic diagram of that apparatus is given in Fig. 1. The negative ion beam is mass-selected and

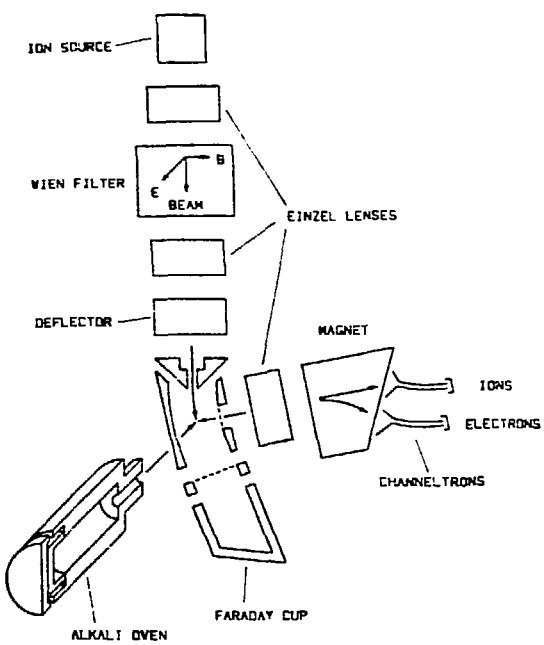

FIG. 1

Schematic diagram of crossed-beam apparatus. The alkali oven (or a gas jet which is not shown) can be rotated into and out of the collision region.

focused into the collision region which is within a one-sixth section of a 127° cylindrical electrostatic energy analyzer. The voltage across the two curved plates of the analyzer allows the ion beam to pass resonantly through the analyzer section. The ion beam intersects, midway of its path inside the analyzer, with a neutral target beam. The electric field maintained across the analyzer is used to extract the slow anions and electrons produced in the collision region through a grid on the inner

plate. The extracted anions and electrons are then focused, separated by a magnetic field and detected with conventional particle multipliers.

The alkali oven, along with a separate gas nozzle identical in shape to the oven's exit cylinder, may be rotated into the collision region. This design enables one to monitor and calibrate the apparatus, before and during experiments with alkali vapors, using some previously studied reactants[5] such as $H^- + O_2$ and $H^- + Ar$. Liquid-nitrogen-cooled surfaces are positioned to trap the undesired alkali vapor. A vexing source of noise is related to the presence of alkali atoms on the surfaces within the collision region. Even with no ion beam in the collision region, some negatively-charged particles are observed to desorb from the alkali-coated surface and arrive at the two particle multipliers. The intensity of these particles increases dramatically as one increases the partial pressure of oxygen or water vapor in the vacuum chamber and, in fact, can easily saturate both particle multipliers. This problem prevents one from using $H^- + O_2$ to calibrate the apparatus during the alkali experiments. These negatively-charged particles which come from alkali-coated surfaces include both electrons and anions; their production mechanism remains unexplained at this time. Fortunately, in the present experimental environment, the extraneous signals caused by the alkali-coated surfaces decrease when the temperature of the oven increased; at the appropriate temperature to do the experiments, these extraneous signals are about one-eighth of the authentic signals. The background contribution due to these particles is measured by steering the ion beam away from the collision region and observing the resultant signals present with a zero-intensity negative ion beam.

III. Results

A. $M^- + X$

Measurements of $\sigma_e(t)$ for collisions of Cs^-, K^- and Na with rare gas (RG) targets reveal a surprising behavior: virtually no detachment is observed until relatively high (~50 eV) center-of-mass collision energies are reached.[2] This is in contradistinction to what has been observed for similar collisions involving another nsns' negative ion, *viz.*, H^-. The onsets for alkali anion detachment are approximately equal to the thresholds for *excitation* observed in collisions of neutral alkali atoms with these same targets.[6] The similarity between the dynamics of the neutral system and that of the negative ion system, together with the observation (at greater energies) of detachment accompanied by excitation of the alkali parent, suggests that electron detachment in the present experiments is mediated by a two-electron process.

Measurements of $\sigma_e(E)$ for the Cs^-+Ar and K^-+Ar systems are shown as a function of relative collision energy in Fig. 2. Data

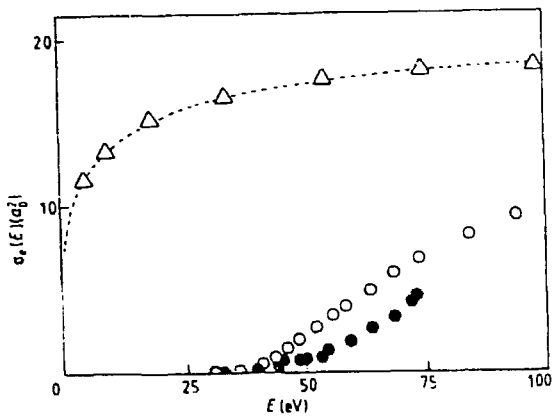

FIG. 2

Total cross sections for electron detachment by Argon; H^- (triangles), K^- (open circles) and Cs^- (solid circles).

for H^-+Ar has been included for comparison. Note that the energetic threshold for detachment of H^- is on the order of a few eV, whereas the thresholds for the K^- and Cs^- projectiles are about 50 eV, approximately 100 times the electron affinity of the alkali atom. A similar result is observed for the Na^-+ Ne system, where the apparent threshold for detachment is about 55 eV. These distinctively high thresholds are typical for the M^- +RG systems where thresholds have been observed. The striking dissimilarity between $\sigma_e(E)$ for M^-+Ar and that for H^-+Ar at these low energies, may be a manifestation of electron correlation. It is well known that H^- is best described by a split shell (1s1s') configuration, implying that the correlation between the two electrons is primarily radial in nature. On the other hand, recent calculations[7] of M^- wave-functions suggest that angular correlation between the valence electrons is significant for the M^- ions. Perhaps it is this difference in character that leads to a difference in the threshold behavior of $\sigma_e(E)$.

An M^-+RG correlation diagram (for the example of Na^-+Ne) is proposed in Fig. 3. The diagram has been inferred in part from

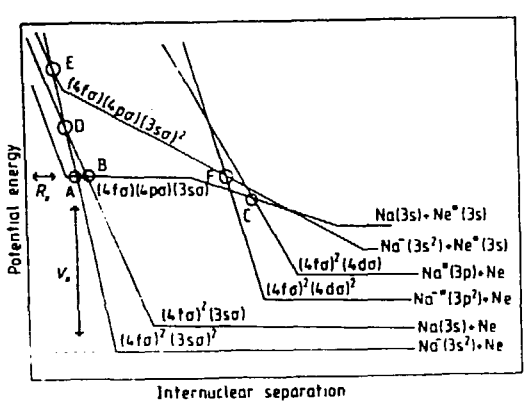

FIG. 3

A schematic representation of molecular configuration correlation diagram for Na + Ne + e.

calculations for the Na+He system[8] and also from the observation of a common threshold for detachment (of Na^-) and of excitation (of both Na and Ne). The incoming Na^-+Ne state remains below the $X^2\Sigma^+$ continuum of Na+Ne+e until the crossing with the continuum of $Na+Ne^*(3s)+e$ is reached at A. This crossing (with coordinates R_X, V_X) accounts for the onset of electron detachment at the collision energy $E = V_X$. A subsequent transition at B can result in ground state products. If one assumes that the probability for detachment at crossing A is unity, then the total cross section is given by

$$\sigma_e(E) = \pi R_X^2(1 - V_X/E) \quad \text{for } E > V_X$$

$$= 0 \quad \text{for } E < V_X.$$

Estimates of R_X and V_X can be made by fitting this expression to the data. The recovered values for the Na^-+Ne system are V_X=65 eV and $R_X = 1.6\ a_o$. The fact that the threshold for Na(3s)+Ne → Na(3P)+Ne is the same as that for detachment of Na^- by Ne suggests that A is located near B. The remarkable agreement between the estimated position of A and the calculated position of B indicates that this picture has some validity.

Measurements of $\sigma_e(E)$ and the cross sections for charge transfer have also been completed for H_2, D_2, N_2, O_2, CO, CO_2, and CH_4 targets. The energetic thresholds for electron detachment are found to be about 5 eV for H_2 and D_2 and range from 3-10 eV for the other molecular targets.

The detachment channel is especially interesting for the CO_2 target. As can be seen in Fig. 4, significant structure is

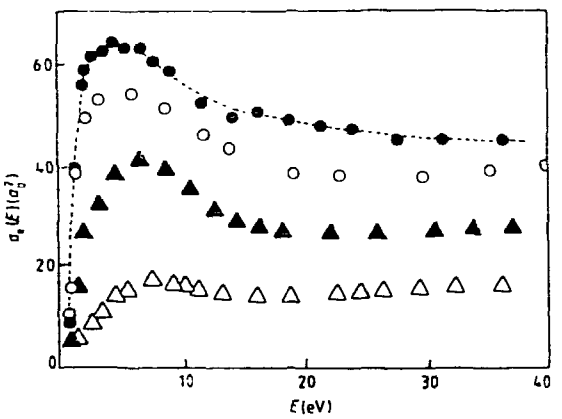

FIG. 4

Detachment cross sections for H^-(Δ), Na^-(▲), K^-(○), and Cs^-(●) + CO_2.

present in $\sigma_e(E)$ for the H^-, Na^-, K^-, and Cs^- projectiles. This structure is peculiar to projectiles possessing two valence s-electrons; O^-, S^-, and halogen anions do not yield this structure for CO_2. The relatively strong dependence on energy of $\sigma_e(E)$ for $E < 15$ eV suggests that the detachment process may occur via a negative-ion resonance of the target. The $CO_2^-(^2\Pi_u)$ shape

resonance, which is an important detachment mechanism in high energy H^-+CO_2 collisions,[9] has an endoergicity of about 4 eV. In contrast, the present measurements of $\sigma_e(E)$ indicate a substantial cross section (~10 Å^2 for K^-+CO_2) at 2 eV. Even after taking into account instrumental and doppler broadening inherent to the experiment, the observed threshold (~1.2 eV) is much lower than is necessary to access the $^2\Pi_u$ state. There is, however, a metastable state of CO_2^- ($^2A_1$) which lies at a lower energy.[10] This state (which has a lifetime of ~90 μs) is bent in its equilibrium geometry with a bond angle of ~135°, and its energy lies approximately 0.7 eV above that of the CO_2 ($^1\Sigma^+_g$) ground state. The endoergicity of charge transfer to this state is therefore about 1.2 eV (0.7 eV plus the electron affinity of the alkali), suggesting that for E < 15 eV, electron detachment is mediated by charge transfer to this metastable $^2A_1$ state of CO_2^-.

For the systems listed above, it is only for the O_2 target that charge transfer is observed to be the dominant electron removal mechanism. In fact, σ_{ct} is as large as 400 a_o^2 for Cs^-+O_2 at E≈4 eV.

B. $H^-(D^-)$ + M

The measured cross sections for charge transfer and electron detachment for collisions of H^- with Na are shown in Fig.5 as

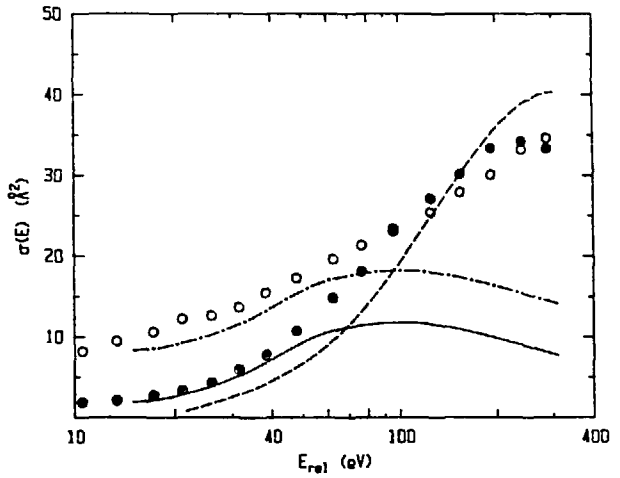

FIG. 5

Charge transfer cross section for H^- + Na - solid circles (exp.) and dashed line (eq. 4); detachment: open circles (exp.) and solid line (eq. 3).

functions of relative collision energy. Since the target thickness in the crossed-beam experiments could not be measured accurately, the absolute value of the cross sections reported here were not experimentally determined. We have chosen to normalize $\sigma_{ct}(E)$ to a calculation of Olson and Liu[11] at high energy in order to facilitate comparison. As may be seen in Fig. 5, the energy dependence of $\sigma_{ct}(E)$ agrees well with this calculation. However, the measured electron detachment cross sections seriously disagree with their prediction that $\sigma_e/\sigma_{ct} \leq 0.5$.

There are several possible reasons for this disagreement; they will be discussed below.

First, it is useful to refer to the potential curves for NaH and NaH^- in Fig.6. These curves are obtained directly from the

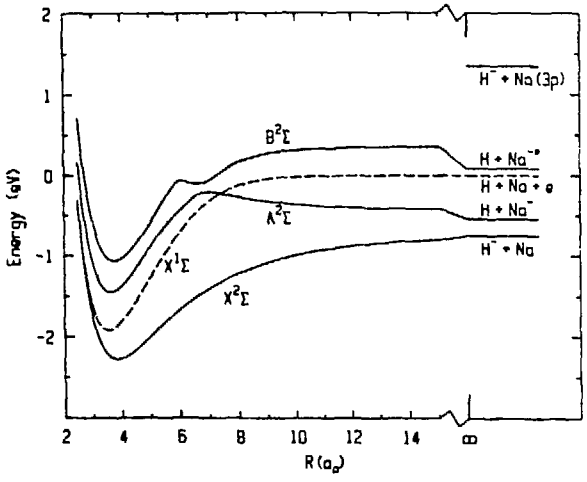

FIG. 6

Low-lying molecular states of NaH^- (solid lines) and ground state of NaH; from Ref. 11.

numerical results reported by Olson and Liu, adjusted to account for the correct electron affinity of hydrogen. As may be seen, the $X^2\Sigma$ state crosses into the $X^1\Sigma$ continuum around $R = 2.7\ a_o$, agreeing with the calculation of Karo et al.[12] This crossing (which was ignored in Ref. 11) will clearly contribute to $\sigma_e(E)$ with a maximum cross section of about 6 $Å^2$.

Second, it is useful to review the two-state PSS calculation for the charge transfer and electron detachment cross sections. In the calculation, as presented in Ref. 11, it is presumed that the electron-loss of H^- is due primarily to a long-range coupling between the $X^2\Sigma$ and $A^2\Sigma$ states. In order to determine a diabatic coupling matrix element between these two states of NaH^-, a point-charge-induced interaction ($\alpha/2R^4$) is assumed for the diabatic curves. By comparing these diabatic curves with the calculated adiabatic $X^2\Sigma$ and $A^2\Sigma$ curves at large internuclear distance ($R = 10 - 20\ a_o$), the diabatic coupling matrix element is found to be:

$$H_{12}(R) = 0.0274 \exp(-0.171R) \qquad (1)$$

Probability evolution on each channel is then calculated by using a two-state PSS method with straight-line trajectories. In that model, the amplitude for the particles to be in the upper $A^2\Sigma$ state is

$$C_2(b,v,x) = (i\hbar v)^{-1} \int_{-\infty}^{x} H_{12} \exp(i\phi)\, dx' \qquad (2)$$

with $$\phi(b,v,x) = (\hbar v)^{-1} \int_{0}^{x} (H_{22} - H_{11})\, dx'$$

in first-order approximation ($C_1 \approx 1$), where H_{11} and H_{22} are the diabatic potential curves, C_1 and C_2 the amplitudes on states $X^2\Sigma$ and $A^2\Sigma$, b is the impact parameter, v the collision velocity and x is vt.

Although detachment directly from $X^2\Sigma$ was neglected, autodetachment from $A^2\Sigma$ was included. As may be seen in Fig.6, the $A^2\Sigma$ state crosses into the $X^1\Sigma$ continuum at $R_2 \approx 7.4\ a_o$. Thus, for trajectories with $b < R_2$, the $A^2\Sigma$ state may yield autodetachment when $R < R_2$. In fact, unit probability was assumed for electron ejection from the $A^2\Sigma$ state at this crossing. In other words, the long-range interaction between the target and the incoming projectile ($t < 0$) on a trajectory with $b < R_2$ yields an electron detachment cross section

$$\sigma_e(v) = \int_0^{R_2} |C_2(b,v,-(R_2^2 - b^2)^{1/2})|^2\ 2\pi b\ db \qquad (3)$$

For $b > R_2$, the coupling leads only to charge transfer. The resultant charge transfer cross section is

$$\sigma_{ct}(v) = \int_{R_2}^{\infty} |C_2(b,v,\infty)|^2\ 2\pi b\ db \qquad (4)$$

The contribution to σ_{ct} for outgoing trajectories (i.e., $t > 0$) on a trajectory with $b < R_2$ is not included in (4). The magnitude of this contribution is uncertain due to a lack of information about the coupling for $R < R_2$.

Numerical calculations using (3) and (4) have been performed and the calculated charge transfer cross sections duplicate those presented in Ref. 11 to within 5%. Yet, we get very different results for electron detachment, viz., $\sigma_e(E)$ is found to be larger than $\sigma_{ct}(E)$ for energies below 70 eV or so, as shown in Fig.5.

The detachment due to the crossing of the $X^2\Sigma$ and $X^1\Sigma$ states, combined with that predicted by (3), can well account for the measured electron detachment cross sections for low energy; this is shown by the dot-dash line in Fig.5. The gap between the dot-dash line and the measured electron detachment cross sections shows an energy dependence similar to the charge transfer cross sections. This strong energy dependence suggests that there exists another electron loss channel that is near resonant in nature.[13]

The exit channels for electron loss discussed so far include only $H + Na^-$ and $H + Na + e$. The energy loss spectra of neutral H

for collisions of H^- + Na, as measured by Tuan and Esaulov,[14] suggest that the Na^{-*} shape resonance[15,16] plays a role comparable to that for charge transfer to Na^-. Of course, Na^{-*} will autodetach and contribute to electron detachment. To the best of our knowledge, no theoretical prediction or explanation exists to account for a substantial production of Na^{-*} in slow collisions of H^- + Na.

To summarize, charge transfer in slow collisions of H^- with Na is due to long-range coupling between $X^2\Sigma$ and $A^2\Sigma$; a previous calculation[11] agrees well with our measurements. For the electron detachment, on the other hand, there are several responsible mechanisms: (1) autodetachment due to the crossing of $X^2\Sigma$ into $X^1\Sigma$; (2) charge transfer to $A^2\Sigma$ for $b < R_2$ and $t < 0$ and thereafter detachment due to the crossing of $A^2\Sigma$ into $X^1\Sigma$; (3) charge transfer to $A^2\Sigma$ in $R < R_2$ and thereafter transition to $B^2\Sigma$ or $H + Na^{-*}$ shape resonance state due to the avoided crossing between $A^2\Sigma$ and $B^2\Sigma$.

The measurements of σ_{ct} and σ_e for collisions of D^- with Na (and H^- + Na) display velocity-dependent isotope effects which are consistent with the theories discussed above; the two-state PSS method with straight-line trajectories inherently contains a velocity-dependent isotope effect for H^- and D^-.

The measurements of σ_{ct} and σ_e for collisions of H^- and D^- with K are shown in Fig.7 as functions of collision velocity.

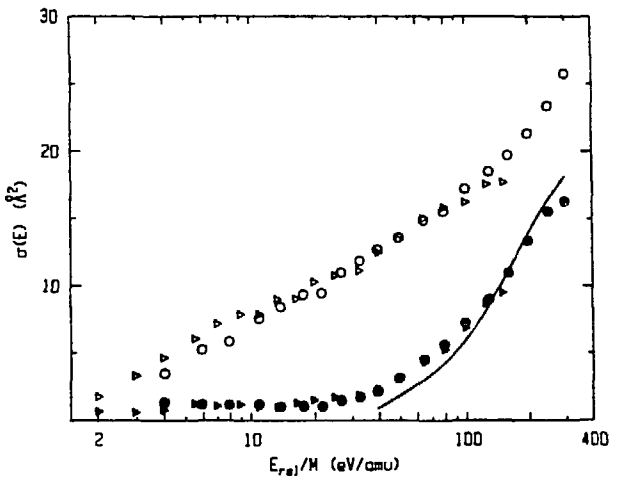

FIG. 7

Charge transfer (solid symbols) and electron detachment (open symbols) for H^- (circles) and D^- (triangles) + K. The solid line is from Ref. 11.

As for Na, we have chosen to normalize the measured σ_{ct} for H^- + K to Olson and Liu's calculation at high energy. As may be seen in the figure, the general structure of σ_{ct} and σ_e for K are very similar to those for Na. This feature suggests that the electron-loss mechanisms are the same for these two targets. The threshold of σ_{ct} for K is higher than that for Na and the overall cross sections for K are smaller than those for Na. These differences

are due to the fact that K has a smaller electron affinity and a larger dipole polarizability, and consequently a larger energy gap between the $X^2\Sigma$ and $A^2\Sigma$ states of KH^-.

In summary, both charge transfer and electron detachment are significant electron-loss mechanisms in slow collisions of H^- and D^- with Na and K. Both processes exhibit a velocity-dependent isotope effect for H^- and D^-. $\sigma_{ct}(E)$ displays a strong energy dependence and high energetic thresholds (about 20 eV for H^- + Na and 40 eV for H^- + K), while $\sigma_e(E)$ displays weaker energy dependence and apparent zero energy thresholds.

Measurements for the reactants $H^-(D^-)$ + Cs are currently underway.

ACKNOWLEDGEMENTS

The work reported in this paper was supported in part by the U. S. Department of Energy, Office of Basic Energy Sciences, Division of Chemical Sciences.

REFERENCES

1. Yu. P. Korchevoi and V. N. Makarchuk, Ukr. Fiz. Zh. 24, 897 (1979).
2. D. Scott, M. S. Huq, R. L. Champion and L. D. Doverspike, Phys. Rev. A 32, 144 (1985).
3. D. Scott, M. S. Huq, R. L. Champion and L. D. Doverspike, Phys. Rev. A 33, 170 (1986).
4. M. S. Huq, L. D. Doverspike and R. L. Champion, Phys. Rev. A 27, 2831 (1983).
5. M. S. Huq, L. D. Doverspike and R. L. Champion, Phys. Rev. A 27, 785 (1983).
6. V. Kempter, B. Kubler and W. Mecklenbrauch, J. Phys. B 7, 2375 (1974); W. Mecklenbrauch, J. Schon, E. Speller and V. Kempter, J. Phys. B 10, 3271 (1977).
7. B. L. Christensen-Dalsgaard, J. Phys. B 18, L407 (1985); J. L.Krause and R. S. Berry, Comment. At. Mol. Phys. 18, 91 (1986).
8. C. Courbin-Gaussorques, P. Wahnon and M. Barat, J. Phys. B 12, 3047 (1979).
9. V. N. Tuan, V. Esaulov and J. P. Gauyacq, J. Phys. B 17, L133 (1984); V. A. Esaulov, J. P. Grouard, R. I. Hall, M. Landau, J. L. Montmagnon, F. Pichou and C. Schermann, J. Phys. B 17, 1855 (1984).
10. R. N. Compton, P. W. Reinhardt and C. D. Cooper, J. Chem. Phys. 63, 3821 (1975).
11. R. E. Olson and B. Liu, J. Chem. Phys. 73, 2817 (1980).
12. A. M. Karo, M. A. Gardner and J. R. Hiskes, J. Chem. Phys. 68, 1942 (1978).
13. J. P. Gauyacq, J. Phys. B 12, L387 (1979).

14. V. N. Tuan and V. A. Esaulov, Phys. Rev. A32, 883 (1985).
15. A. R. Johnston and P. D. Burrow, J. Phys. B 15, L745 (1982).
16. A. L. Sinfailam and R. K. Nesbet Phys. Rev. A 7, 1987 (1973).